Machine learning accelerated discovery of low-Pt high entropy intermetallic compounds for electrochemical oxygen reduction reaction

Longhai Zhang[‡, #], Jiaxi Zhang[‡, #], Changsheng Chen[⊥, #], Weiquan Tan[‡], Xu Zhang[▽], Li Du[‡], Huiyu Song[‡], Shijun Liao[‡], Ye Zhu[⊥, *] and Zhiming Cui[‡, *]

[‡]The Key Laboratory of Fuel Cell Technology of Guangdong Province, School of Chemistry and Chemical Engineering, South China University of Technology, Guangzhou 510641, China.

[⊥]Department of Applied Physics, Research Institute for Smart Energy, The Hong Kong Polytechnic University, Hong Kong, 999077, China.

[▽]School of Chemical Engineering, Zhengzhou University, Zhengzhou 450001, China.

[#]These authors contributed equally to this work.

KEYWORDS: Machine learning; low-Pt; high entropy intermetallic compounds; oxygen reduction reaction

ABSTRACT: Advancing the design of novel cathode catalysts to significantly minimize platinum utilization and augment the longevity of the catalyst has emerged as a formidable challenge in the field of fuel cells. Here, the PtM_3 type low-Pt high entropy intermetallic (HEI) with ultra-high efficiency is first demonstrated as a class of advanced electrocatalyst for oxygen reduction reaction. Machine learning techniques using crystal graph convolutional neural networks (CGCNN) was employed to expedite the composition design, which can hardly be achieved by massive trail-and-error efforts. By training the CGCNN model on a dataset generated from first-principles calculations, a high accuracy with a mean absolute error (MAE) of 0.002 for surface strain and 0.282 eV for formation energy is achieved. Further, the HEI $PtFe_{0.75}Co_{0.75}Ni_{0.75}Cu_{0.75}$ with PtM_3 type structure was predicted to be a prossing ORR catalyst and was successfully synthesied with nanoparticle sizes around 6 nm, which demonstrates a mass activity of 4.09 A mg Pt^{-1} and a specific activity of 7.92 mA cm^{-2}, as well as significantly enhanced stability.

Discovery of advanced electrocatalysts for oxygen reduction reaction (ORR) is crucial for the development of proton exchange membrane fuel cells (PEMFCs).[1] Because the ORR has a four-proton-coupled electron transfer process, it usually suffers from a high over potential to overcome its kinetic barrier.[2-3] Pt/C is still the state of art ORR catalyst but high Pt loading on membrane is needed to provide enough power density because of its limited activity. The scarce resources and increased cost of Pt have led to extensive research to reduce the amount of Pt in a catalyst without compromising its performance.[4] Structurally ordered Pt-based intermetallic compounds (ICs) have recently evolved as a class of promising ORR catalysts due to their well-defined crystal structure, stoichiometry, improved catalytic efficiency, and stability compared to their random alloy counterparts.[5-7] Specifically, $L1_2$ type intermetallic Pt_3Cr,[8] Pt_3Mn,[9] Pt_3Co[10] and Pt_3In[11] as well as $L1_0$ type intermetallic PtFe,[12] PtCo,[13-14] PtNi[15] and PtZn[16] have shown superior ORR activity and stability on half-cell or single cell. Moreover, many efforts have been devoted to tune the composition of the intermetallics thus to further enhance the ORR performance.[17-20] Apart from the widely reported Pt-richer intermetallic Pt_3M and PtM, the low-Pt intermetallic PtM_3 have also attracted some research interests.[21-24] Especially, Yang's work shows that $PtCu_3$ can exert biggest surface strain on the actively constructed surface Pt layer and exhibit best specific activity (SA) and mass activity (MA) among the intermetallics library,[25] indicating the potential of low-Pt ICs been applied in PEMFCs. However, due to the increase of non-nobel metals, the stability of the intermetallic structure has a greater impact on the electrochemical performance of PtM_3. Specifically, the 5d-3d interactions of Pt-M in PtM_3 are less than those in Pt_3M and PtM due to that the coordination numbers of Pt and M are much less than those in Pt_3M and PtM. With the decrease of Pt-M interactions, the leaching of M gets easier. Besides, the formation energy of intermetallic PtM_3 is generally higher than those of Pt_3M and PtM, indicating the lower thermodynamic stability of intermetallic PtM_3, which would further lead to the uneven size distribution of nanoparticles during the essential high temperature annealing process.

Recently, the emerging high entropy intermetallics (HEIs), which usually consist of five or more element and specific crystal structure inherited from parent binary intermetallics, have witnessed significant achievements in catalysis.[26-28] The HEIs not only provide a wider range of component

modulation compared with binary and ternary ICs, but also possess unique structure stability benifiting from the sluggish diffusion and high entropy effects.[29-31] To this end, extending low-platinum intermetallics to HEIs could increase the possibility of discovering more advanced oxygen reduction catalysts. Nevertheless, It is still a formidable challenge for the component design of HEIs because the traditional trial-and-error process can hardly realize the target due to the huge space of element and ratio. Machine learning (ML) technique has achieved significant success in accelerating the discovery and screening of electrocatalysts.[32-34] The ML algorithms with multiple processing layers can provide insight into complex, multidimensional structure-property relations, thus complementing the expensive, time and resource-dependent density functional calculations of electronic structure.[35-37] Among the developed ML framework, the crystal graph convolutional neural networks (CGCNN) developed by Xie and Grossman provide a universal and interpretable representation of periodic crystal systems and can directly learn material properties from the connection of atoms in the crystal.[38] The model could achieve a mean absolute error (MAE) of 39 meV $atom^{-1}$ for the prediction of formation energy (E_f) with the dataset taken from the Materials Project.[39] Combining CGCNN and DFT derived basic crystal properties has the potential to predict the promising low-Pt HEIs for ORR, yet still lack relevant research.

Herein, based on intermetallic $PtCu_3$ and $PtFe_3$, different transition metal replaced crystals with variable atomic ratio in sublattice were constructed and 364 sets of DFT calculated structure-properties data were obtained. The dataset was used to train the CGCNN model for predicting the surface strain and E_f of the other designed low-Pt ICs. The MAE achieved here for surface strain and E_f is 0.002 and 0.282 eV, respectively. The predicted results show that $PtCu_{1.5}Co_{1.5}$, $PtCu_{1.5}Ni_{1.5}$, $PtFe_{1.5}Co_{1.5}$ and $PtFe_{1.5}Ni_{1.5}$ would be the highly efficient ORR electrocatalysts. Then the facile freeze-drying-thermal reduction method was employed to prepare the ternary, quaternary and quinary low-Pt ICs tentatively. The as prepared carbon supported HEI of $PtFe_{0.75}Co_{0.75}Ni_{0.75}Cu_{0.75}$/C possesses a SA of 7.92 mA cm^{-2} and a MA of 4.09 A mg Pt^{-1}, which is much higher than most of the other reported low-Pt intermetallics.

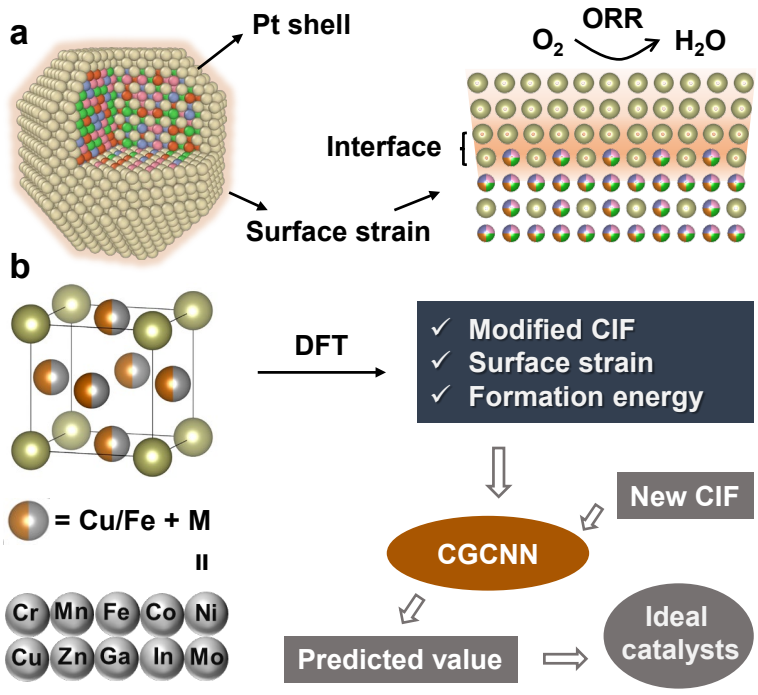

Figure 1. (a) The illustration of the surface strain originated from the lattice mismatch of the interface between the intermetallic/alloy core and Pt shell. (b) The schematic illustration of the machine learning guided element selection toward low-Pt ORR catalysts process.

Generally, before serving as the cathodic catalysts in PEMFCs, a tight Pt shell with three or more atomic layers would be constructed on the Pt based nanocrystals, which can improve the Pt utilization and protect the alloy core to some extent. In this way, the strain effect, specifically the lattice strain, anisotropic strain or surface strain, plays a dominated role in modulating the adsorption and dissociation of oxygen reduction reaction intermediate species, thus influencing the reaction kinetics.[6, 19, 25, 40] The surface strain of Pt-based ICs originates from the lattice mismatch of the interface between the intermetallic core and Pt shell and can be obtained from their lattice parameters (**Figure 1a**). It has been reported that surface strain has a good linear relationship with oxygen reduction performance. Besides, the formation energy (E_f) is a thermodynamic property of an alloy, which is related to the stability of the metallic catalysts. Hence, the surface strain and E_f were employed as the target value for ML process. **Figure 1b** shows the DFT based and ML accelerated element selection process for ideal ORR catalysts. The base materials are the most reported $PtCu_3$ and $PtFe_3$ while the substitution elements include the 3d transition metals near the Fe/Cu and the Ga/In/Mo, which have been reported to modify the ORR performance of Pt based alloy. The element ratio of non-Pt element in the trimetallic ICs includes 1:1, 2:1, 3:1, and 5:1. After the DFT calculations, the lattice parameters and energy of the models can be obtained which can be used to calculate the surface strain and E_f, respectively. The details of model construction, DFT calculations and target value calculations are described in the **Computational details** of **Supporting Information (SI)**. Before training the CGCNN model, the CIF files of the DFT optimized structures were modified, in which the lattice parameters were replaced by the average values of all the optimized structures. The details of ML process are described in the **Machine learning details** of **SI**.

Based on intermetallic $PtFe_3$ and $PtCu_3$, 364 sets of structure-properties data were obtained, forming the dataset for training the CGCNN model. Figure 1 shows the good linear relationship between predicted values versus calculated values for the CGCNN model after being trained. The R^2 and the mean absolute error (MAE) for E_f are 0.983 and 0.282 eV, respectively. As for surface strain, the R^2 and MAE are 0.994 and 0.002, respectively, which means that the CGCNN model is more accurate in predicting the lattice parameters. Actually, $PtMn_3$ is also a kind of IC that have been reported in the field of catalysis.[41] When the $PtMn_3$ was considered as a main structure, together with $PtFe_3$ and $PtCu_3$, a dataset of 563 sets of data can be obtained. However, the CGCNN model trained with this dataset give a worse predictive accuracy than before (**Figure S1**). The R^2 and MAE are 0.939 and 0.500 eV for E_f, respectively. The R^2 and MAE are 0.952 and 0.006 for surface strain, respectively. Similarly, the prediction of surface strain is also more accurate than that of E_f. To distinguish the factors influencing the model, the data in **Figure S1** were labeled and presented in **Figure S2**. It can be found that the data away from the fitting line almost belong to the trimetallic alloys in which the Mn is more than the other non-Pt atoms. This indicting the properties of $PtMn_3$ based systems are more difficult to be predicted precisely, especially the E_f. This may be caused by the errors of energy obtained by simple DFT calculations, because the electron spin has a great influence on the energy of $PtMn_3$ based ICs.

In addition, in order to explore the predictive ability of the CGCNN model with a small sample size, 100 sets of data randomly selected from the initial dataset were used to train the CGCNN model. **Figure S3** shows that the R^2 and MAE can still be maintained at 0.950 and 0.423 eV for E_f, 0.992 and 0.002 for surface strain, respectively. To this end, the CGCNN model have great potential in properties prediction for ICs based on small DFT obtained dataset, which means it can reduce the time-consuming DFT calculations.

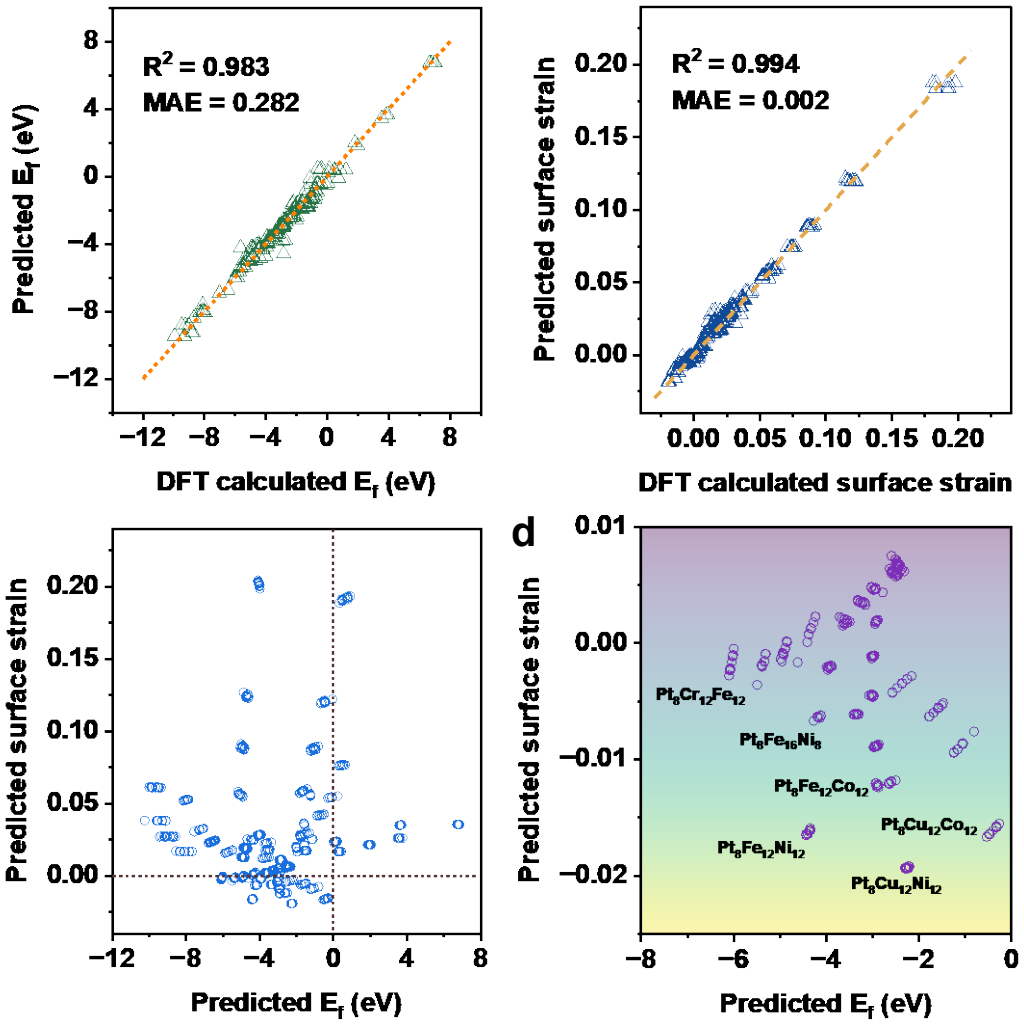

Figure 2. Predicted versus calculated values for the CGCNN models after being trained. (a) formation energy (E_f); (b) surface strain; (c) Predicted values of formation energy (E_f) and surface strain; (d) Enlarged area of (c) where Ef < 0 and surface strain < 0.01.

Further, more $PtFe_3$ and $PtCu_3$ based model (~800) were constructed and the CIF files were obtained and modified. The CGCNN models after being trained was used to predict the E_f and surface strain of above unoptimized models. The results are plotted in **Figure 2a**. The gathered data points belong to the trimetallic structures with same atom and atom ratio but different atomic arrangement in sublattice. This means that the different atomic occupancy does not cause large changes in structure properties. With the objective of identifying and synthesizing advanced low Pt intermetallic catalysts for the ORR, we have focused on the enlarged region in Figure 2d where the E_f is less than 0 and the surface strain is negative. As can be seen in **Figure 2b**, the $PtFe_{1.5}Co_{1.5}$, $PtFe_{1.5}Ni_{1.5}$, $PtCu_{1.5}Co_{1.5}$, and $PtCu_{1.5}Ni_{1.5}$ possess quite negative surface strain. Because the surface strain is calculated relative to $PtCu_3$, the Co and Ni with half substitution are the optimal selection for enhancing the ORR electrocatalysis. On the contrary, from the area where $E_f < 0$ and surface strain > 0 (**Figure S4**), $PtCu_{1.5}Ga_{1.5}$, $PtCu_{1.5}In_{1.5}$ and $PtCu_{1.5}Cr_{1.5}$ are predicted to show worse ORR activity than $PtCu_3$.

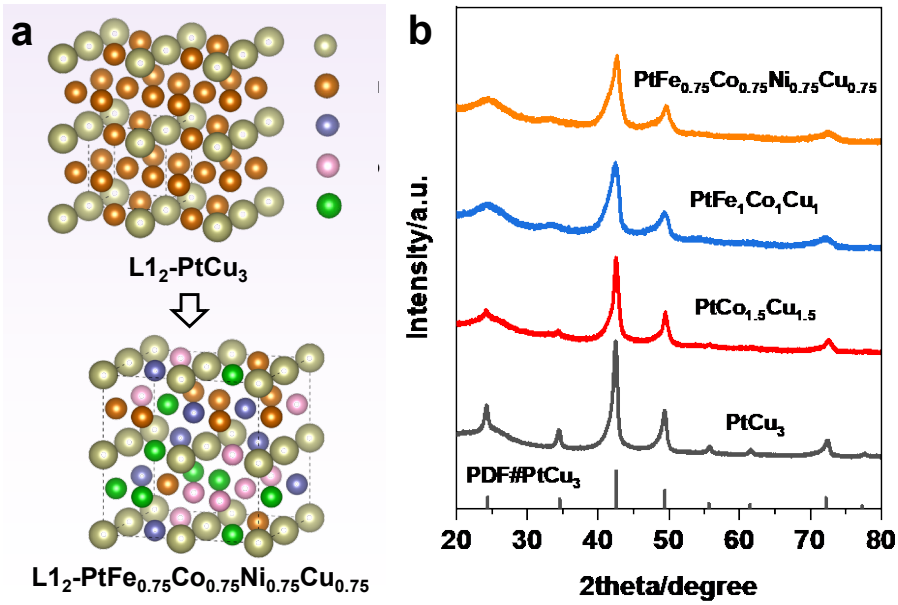

Figure 3. (a) Atomic structure models of intermetallic $PtCu_3$ and $PtFe_{0.75}Co_{0.75}Ni_{0.75}Cu_{0.75}$; (b) XRD patterns of carbon supported catalysts.

According to the results of DFT based ML process, the ternary, quaternary or quinary Pt-based ICs were expected to be synthesized containing Cu, Fe, Co and Ni with equal atomic ratio distributed in non-Pt sublattice. Figure 3a shows the structures of intermetallic $PtCu_3$ and $PtFe_{0.75}Co_{0.75}Ni_{0.75}Cu_{0.75}$. The facile freeze-drying-thermal reduction method was employed and the details can be found in the **Materials synthesis** section of the **SI**. X-ray diffraction (XRD) was employed to characterize the phase of different products. **Figure 3b and Figure S5** show the XRD patterns. For $PtCu_3$ based ICs, the peaks of XRD are similar to that of $PtCu_3$ of which the peaks at ~24° and ~34° correspond to the super lattice of intermetallics.[23] To this end, $PtCu_3$, $PtCu_{1.5}Co_{1.5}$, $PtFe_{1.5}Co_{1.5}$, $PtFe_{1.5}Ni_{1.5}$, $PtCu_1Fe_1Co_1$, $PtCu_1Fe_1Ni_1$, $PtFe_1Co_1Ni_1$ and $PtFe_{0.75}Co_{0.75}Ni_{0.75}Cu_{0.75}$ present intermetallic phase. Fast-Thermal-shock method was adopted to synthesize $PtFe_{0.75}Co_{0.75}Ni_{0.75}Cu_{0.75}$ solid solution.[42] The XRD patterns in **Figure S6** shows the left shifted peaks and disappeared superlattice peaks of solid solution relative to the as synthesized $PtFe_{0.75}Co_{0.75}Ni_{0.75}Cu_{0.75}$, further verified the formation of intermetallic phase. The atomic arrangement of Pt and Fe/Co/Ni/Cu can be characterized by high-angle annular dark-field scanning transmission electron microscopy (HAADF-STEM). Figure 4a shows the HAADF-STEM image of a $PtFe_{0.75}Co_{0.75}Ni_{0.75}Cu_{0.75}$ nanoparticle. The ordered bright and dark columns are Pt and Fe/Co/Ni/Cu atoms, respectively, indicating the ordered atomic arrangement. The corresponding fast fourier transform (FFT) in Figure 4b exhibits 001 and 110 diffraction spots, which should be extinct fort he face-centered cubic structure, providing further evidence of the ordering in $PtFe_{0.75}Co_{0.75}Ni_{0.75}Cu_{0.75}$. The atom columns in Figure 4c shows that each unit cell is composed of a rectangular array consisting of pure Pt columns at the center and Fe/Co/Ni/Cu columns at the corners, consistent with the crystal structure model. The energy-dispersive X-ray spectroscopy (EDS) mapping shows a uniform element distribution in the $PtFe_{0.75}Co_{0.75}Ni_{0.75}Cu_{0.75}$ nanoparticle. For nanocatalysts, small nanoparticle size is beneficial to exhibit high mass activity. Since the half peak width of XRD is positively correlated with the particle size of the synthesized nanomaterials and the wider the half peak width, the smaller the nanoparticles, the as synthesized $PtCu_3$, $PtCu_{1.5}Co_{1.5}$, $PtCu_1Fe_1Co_1$ and $PtFe_{0.75}Co_{0.75}Ni_{0.75}Cu_{0.75}$ were selected for further study to validate previous predictions and identify practical ORR catalysts. However, the XRD of $PtCu_{1.5}Ga_{1.5}$, $PtCu_{1.5}In_{1.5}$ and $PtCu_{1.5}Cr_{1.5}$ shows mixed phase (**Figure S7**), indicating that the phase formation of multicomponent intermetallic compound is not only determined by thermodynamic E_f.

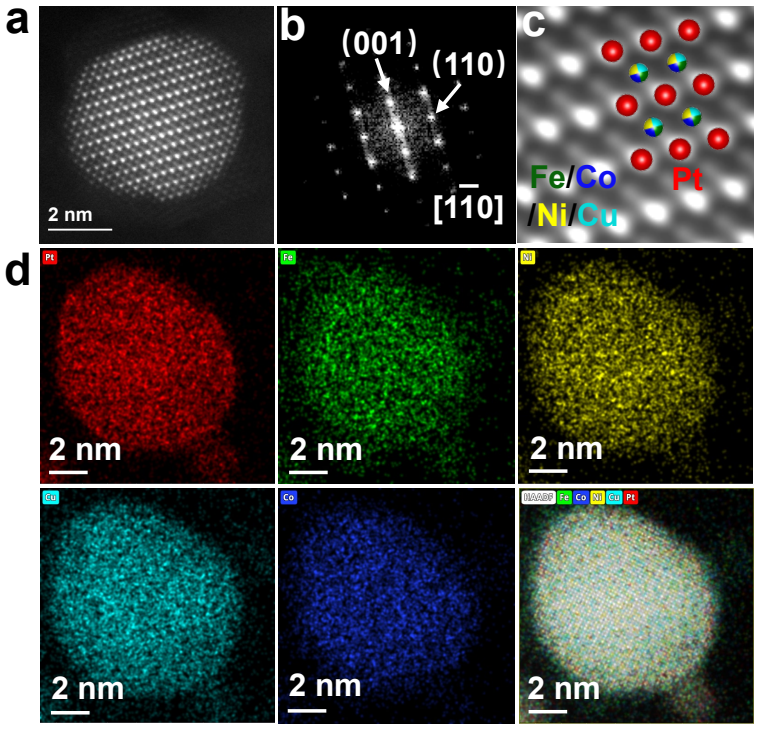

Figure 4. (a) HAADF-STEM image, (b) FFT, (c) atomic structure model of $PtFe_{0.75}Co_{0.75}Ni_{0.75}Cu_{0.75}$ superposed on the HAADF-STEM image and (d) EDS mapping of the $PtFe_{0.75}Co_{0.75}Ni_{0.75}Cu_{0.75}$ nanoparticle.

Cyclic voltammetry (CV) and linear scanning voltammetry (LSV) were used to evaluate the ORR performance of the above electrocatalysts. First, an electrochemical dealloying process involving multiple CV cycles with a sweep rate of 0.2 V s^{-1} was conducted for each catalyst and the changes were recorded and shown in **figure S8**. During the dealloying process, the area of H_{ad} desorption peak will become larger and larger until being stable. For $PtCu_3$, after 300 CV cycles, the oxidation/reduction peak of Cu almost disappeared and the oxidation/reduction peak of Pt was revealed. Differently, for $PtFe_{0.75}Co_{0.75}Ni_{0.75}Cu_{0.75}$, only 80~90 CV cycles are needed to achieve the dealloying changes. It is most likely due to the fact that the multi-metal suppressed the surface segregation of non-noble metals, unlike that in $PtCu_3$. After surface dealloying, CV cycles with a sweep rate of 0.05 V s^{-1} was used to measure the electrocatalytic surface area (ECSA) of the catalysts (**Figure 4a**), The ECSA for $PtCu_3$, $PtCu_{1.5}Co_{1.5}$, $PtCu_1Fe_1Co_1$ and $PtFe_{0.75}Co_{0.75}Ni_{0.75}Cu_{0.75}$ are 227.7, 288.6, 900.2 and 516.8 cm^2 mg^{-1}. This indicates that the nanoparticle sizes of $PtCu_1Fe_1Co_1$ and $PtFe_{0.75}Co_{0.75}Ni_{0.75}Cu_{0.75}$ are obviously smaller than that of $PtCu_3$, $PtCu_{1.5}Co_{1.5}$, which is consistent with the result of XRD. LSV was used to test the ORR activity of the catalysts. **Figure 4b** shows the apparent activity of $PtCu_1Fe_1Co_1$ and $PtFe_{0.75}Co_{0.75}Ni_{0.75}Cu_{0.75}$ and is better than that of $PtCu_3$, $PtCu_{1.5}Co_{1.5}$. Further, the MA and SA at 0.9 V vs. RHE were calculated and presented in **Figure 4c**. The MA for $PtFe_{0.75}Co_{0.75}Ni_{0.75}Cu_{0.75}$ and $PtCu_1Fe_1Co_1$ are 4.09 and 3.98 A mg^{-1}_{Pt}, which are much higher than those for $PtCu_3$ (0.96 A mg^{-1}_{Pt}) and $PtCu_{1.5}Co_{1.5}$ (1.77 A mg^{-1}_{Pt}). As for the SA, the positive order is $PtCu_3$ (4.2 mA cm^{-2}) < $PtCu_1Fe_1Co_1$ (4.4 mA cm^{-2}) < $PtCu_{1.5}Co_{1.5}$ (6.09 mA cm^{-2}) < $PtFe_{0.75}Co_{0.75}Ni_{0.75}Cu_{0.75}$ (7.92 mA cm^{-2}). It can be seen that the advantage of size makes the $PtCu_1Fe_1Co_1$ have a small SA, but the MA is very large. Besides, the activity of $PtFe_{0.75}Co_{0.75}Ni_{0.75}Cu_{0.75}$ is much higher than that of most of the other reported low-Pt ICs (Table S1). **Figure S9** shows the LSV curves before and after stability tests. After 5000 accelerated CV cycles, $PtFe_{0.75}Co_{0.75}Ni_{0.75}Cu_{0.75}$ shows an 11-mV decline of half-wave potential, while $PtCu_3$ shows a 23-mV decline, indicating a better stability of $PtFe_{0.75}Co_{0.75}Ni_{0.75}Cu_{0.75}$. TEM images (**Figure S10-S12**) show that the nanoparticles of $PtFe_{0.75}Co_{0.75}Ni_{0.75}Cu_{0.75}$ are about 6.5 nm and maintained well after stability test, while the nanoparticles of $PtCu_3$ occurred serious aggregation. Moreover, the surface

strain of the intermetallic catalysts was calculated by DFT. The average surface strain and SA of the catalysts were matched in **Figure 4d**. A positive relationship is observed, which means that the surface strain does a good descriptor for the intermetallic ORR catalysts, and the ML predictions get experimentally verified.

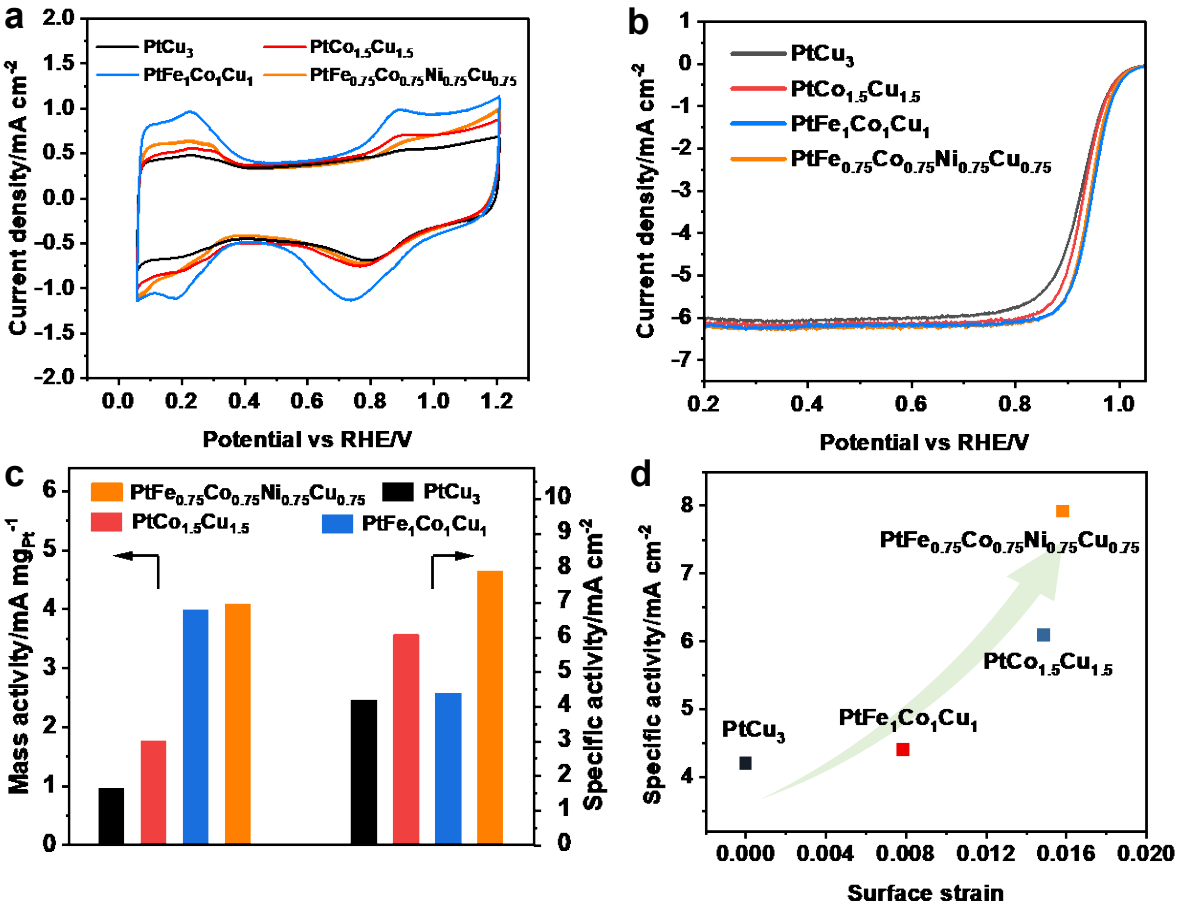

Figure 5. (a) CV curves recorded in N_2 saturated 0.1 M $HClO_4$; (b) LSV curves recorded in O_2 saturated 0.1 M $HClO_4$ at 1600 rpm and 10 mV s^{-1}; (c) mass activity and specific activity of catalysts; (d) the relationship of SA and surface strain.

In summary, this work demonstrated a DFT based, ML accelerated strategy for the discovery of advanced low Pt ORR catalysts. A dataset comprising 364 sets of DFT calculated structure-properties data is generatedbased on the partially substituted $PtFe_3$ and $PtCu_3$. The dataset was used to train the CGCNN model for predicting the surface strain and E_f of the other designed low-Pt ICs. The achieved MAE for surface strain and E_f is 0.002 and 0.282 eV, respectively. The predicted results show that $PtCu_{1.5}Co_{1.5}$, $PtCu_{1.5}Ni_{1.5}$, $PtFe_{1.5}Co_{1.5}$ and $PtFe_{1.5}Ni_{1.5}$ would behighly efficient ORR electrocatalysts. Subsequently, a facile freeze-drying-thermal reduction method was employed to tentatively prepare the ternary, quaternary and quinary low-Pt ICs. Among them, the carbon supported HEI of $PtFe_{0.75}Co_{0.75}Ni_{0.75}Cu_{0.75}$/C exhibits a SA of 7.92 mA cm^{-2} and a MA of 4.09 A mg_{Pt}^{-1}, surpassing most of the reported low-Pt intermetallics. Besides, the SA and surface strain of the investigated intermetallic catalysts shows a positive relationship, confirming the experimental verification of the ML predictions.

ASSOCIATED CONTENT

Supporting Information. Materials and experimental details; Characterizations; DFT calculations. This material is available free of charge via the Internet at http://pubs.acs.org.

AUTHOR INFORMATION

Corresponding Author

Zhiming Cui − The Key Laboratory of Fuel Cell Technology of Guangdong Province, School of Chemistry and Chemical Engineering, South China University of Technology, Guangzhou 510641, China; E-mail: zmcui@scut.edu.cn
Ye Zhu − Department of Applied Physics, Research Institute for Smart Energy, The Hong Kong Polytechnic University, Hong Kong 999077, China; Email: yezhu@polyu.edu.hk

Author Contributions

The authors declare no competing financial interest.

Notes

The authors declare no competing financial interest.

ACKNOWLEDGMENT

This work was supported by the National Natural Science Foundation of China (Project No. 22072048), the Guangdong Provincial Department of Science and Technology (Project No. 2021A1515010128，2022A0505050013) and Guangdong Basic and Applied Basic Research Foundation (Project No. 2022A1515111097).

REFERENCES

(1) Sun, Y.; Polani, S.; Luo, F.; Ott, S.; Strasser, P.; Dionigi, F., Advancements in cathode catalyst and cathode layer design for proton exchange membrane fuel cells. *Nat. Commun.* **2021,** *12*, 5984.
(2) Kodama, K.; Nagai, T.; Kuwaki, A.; Jinnouchi, R.; Morimoto, Y., Challenges in applying highly active Pt-based nanostructured catalysts for oxygen reduction reactions to fuel cell vehicles. *Nat. Nanotechnol.* **2021,** *16*, 140-147.
(3) Li, J.; Sun, S., Intermetallic Nanoparticles: Synthetic Control and Their Enhanced Electrocatalysis. *Acc. Chem. Res.* **2019,** *52*, 2015-2025.
(4) Tang, M.; Zhang, S.; Chen, S., Pt utilization in proton exchange membrane fuel cells: structure impacting factors and mechanistic insights. *Chem. Soc. Rev.* **2022,** *51*, 1529-1546.
(5) Gamler, J. T. L.; Ashberry, H. M.; Skrabalak, S. E.; Koczkur, K. M., Random Alloyed versus Intermetallic Nanoparticles: A Comparison of Electrocatalytic Performance. *Adv. Mater.* **2018,** *30*, 1801563.
(6) Liang, J.; Ma, F.; Hwang, S.; Wang, X.; Sokolowski, J.; Li, Q.; Wu, G.; Su, D., Atomic Arrangement Engineering of Metallic Nanocrystals for Energy-Conversion Electrocatalysis. *Joule* **2019,** *3*, 956-991.
(7) Yan, Y.; Du, J. S.; Gilroy, K. D.; Yang, D.; Xia, Y.; Zhang, H., Intermetallic Nanocrystals: Syntheses and Catalytic Applications. *Adv. Mater.* **2017,** *29*, 1605997.
(8) Cui, Z.; Chen, H.; Zhou, W.; Zhao, M.; DiSalvo, F. J., Structurally Ordered Pt3Cr as Oxygen Reduction Electrocatalyst: Ordering Control and Origin of Enhanced Stability. *Chem. Mater.* **2015,** *27*, 7538-7545.
(9) Zhang, B.; Fu, G.; Li, Y.; Liang, L.; Grundish, N. S.; Tang, Y.; Goodenough, J. B.; Cui, Z., General Strategy for Synthesis of Ordered Pt3 M Intermetallics with Ultrasmall Particle Size. *Angew. Chem. Int. Ed. Engl* **2020,** *59*, 7857-7863.
(10) Wang, X. X.; Hwang, S.; Pan, Y. T.; Chen, K.; He, Y.; Karakalos, S.; Zhang, H.; Spendelow, J. S.; Su, D.; Wu, G., Ordered Pt3Co Intermetallic Nanoparticles Derived from Metal-Organic Frameworks for Oxygen Reduction. *Nano Lett.* **2018,** *18*, 4163-4171.
(11) Wang, Q.; Zhao, Z. L.; Zhang, Z.; Feng, T.; Zhong, R.; Xu, H.; Pantelides, S. T.; Gu, M., Sub-3 nm Intermetallic Ordered Pt_3In Clusters for Oxygen Reduction Reaction. *Adv. Sci.* **2020,** *7*, 1901279.
(12) Li, J.; Xi, Z.; Pan, Y. T.; Spendelow, J. S.; Duchesne, P. N.; Su, D.; Li, Q.; Yu, C.; Yin, Z.; Shen, B.; Kim, Y. S.; Zhang, P.; Sun, S., Fe Stabilization by Intermetallic L10-FePt and Pt Catalysis Enhancement in L10-FePt/Pt Nanoparticles for Efficient Oxygen Reduction Reaction in Fuel Cells. *J. Am. Chem. Soc.* **2018,** *140*, 2926-2932.
(13) Li, J.; Sharma, S.; Liu, X.; Pan, Y.-T.; Spendelow, J. S.; Chi, M.; Jia, Y.; Zhang, P.; Cullen, D. A.; Xi, Z.; Lin, H.; Yin, Z.; Shen, B.; Muzzio, M.; Yu, C.; Kim, Y. S.; Peterson, A. A.; More, K. L.; Zhu, H.; Sun, S., Hard-Magnet L10-CoPt Nanoparticles Advance Fuel Cell Catalysis. *Joule* **2019,** *3*, 124-135.
(14) Xie, M.; Lyu, Z.; Chen, R.; Shen, M.; Cao, Z.; Xia, Y., Pt-Co@Pt Octahedral Nanocrystals: Enhancing Their Activity and Durability toward Oxygen Reduction with an Intermetallic Core and an Ultrathin Shell. *J. Am. Chem. Soc.* **2021,** *143*, 8509-8518.
(15) Zou, L.; Fan, J.; Zhou, Y.; Wang, C.; Li, J.; Zou, Z.; Yang, H., Conversion of PtNi alloy from disordered to ordered for enhanced activity and durability in methanol-tolerant oxygen reduction reactions. *Nano Res.* **2015,** *8*, 2777-2788.
(16) Liang, J.; Zhao, Z.; Li, N.; Wang, X.; Li, S.; Liu, X.; Wang, T.; Lu, G.; Wang, D.; Hwang, B.-J.; Huang, Y.; Su, D.; Li, Q., Biaxial Strains Mediated Oxygen Reduction Electrocatalysis on Fenton Reaction Resistant L10-PtZn Fuel Cell Cathode. *Adv. Energy Mater.* **2020,** *10*, 2000179.
(17) Zhang, J.; Zhang, L.; Cui, Z., Strategies to Enhance the Electrochemical Performances of Pt-based Intermetallic catalysts. *Chem. Commun.* **2021,** *57*, 11-26.
(18) Kim, J.; Hong, Y.; Lee, K.; Kim, J. Y., Highly Stable Pt-Based Ternary Systems for Oxygen Reduction Reaction in Acidic Electrolytes. *Adv. Energy Mater.* **2020,** *10*.
(19) Li, J.; Sharma, S.; Wei, K.; Chen, Z.; Morris, D.; Lin, H.; Zeng, C.; Chi, M.; Yin, Z.; Muzzio, M.; Shen, M.; Zhang, P.; Peterson, A. A.; Sun, S., Anisotropic Strain Tuning of L10 Ternary Nanoparticles for Oxygen Reduction. *J. Am. Chem. Soc.* **2020,** *142*, 19209-19216.
(20) Zhao, W.; Chi, B.; Liang, L.; Yang, P.; Zhang, W.; Ge, X.; Wang, L.; Cui, Z.; Liao, S., Optimizing the Electronic Structure of Ordered Pt–Co–Ti Ternary Intermetallic Catalyst to Boost Acidic Oxygen Reduction. *ACS Catal.* **2022,** *12*, 7571-7578.

(21) Wang, Z.; Yao, X.; Kang, Y.; Miao, L.; Xia, D.; Gan, L., Structurally Ordered Low-Pt Intermetallic Electrocatalysts toward Durably High Oxygen Reduction Reaction Activity. *Adv. Funct. Mater.* **2019,** *29*.
(22) Cui, Z.; Fu, G.; Li, Y.; Goodenough, J. B., Ni3 FeN-Supported Fe3 Pt Intermetallic Nanoalloy as a High-Performance Bifunctional Catalyst for Metal-Air Batteries. *Angew Chem Int Ed Engl* **2017,** *56*, 9901-9905.
(23) Wang, D.; Yu, Y.; Xin, H. L.; Hovden, R.; Ercius, P.; Mundy, J. A.; Chen, H.; Richard, J. H.; Muller, D. A.; DiSalvo, F. J.; Abruna, H. D., Tuning oxygen reduction reaction activity via controllable dealloying: a model study of ordered Cu3Pt/C intermetallic nanocatalysts. *Nano Lett.* **2012,** *12*, 5230-5238.
(24) Wang, S.; Luo, Q.; Zhu, Y.; Tang, S.; Du, Y., Facile Synthesis of Quaternary Structurally Ordered L12-Pt(Fe, Co, Ni)3 Nanoparticles with Low Content of Platinum as Efficient Oxygen Reduction Reaction Electrocatalysts. *ACS Omega* **2019,** *4*, 17894-17902.
(25) Yang, C. L.; Wang, L. N.; Yin, P.; Liu, J.; Chen, M. X.; Yan, Q. Q.; Wang, Z. S.; Xu, S. L.; Chu, S. Q.; Cui, C.; Ju, H.; Zhu, J.; Lin, Y.; Shui, J.; Liang, H. W., Sulfur-anchoring synthesis of platinum intermetallic nanoparticle catalysts for fuel cells. *Science* **2021,** *374*, 459-464.
(26) Cui, M.; Yang, C.; Hwang, S.; Yang, M.; Overa, S.; Dong, Q.; Yao, Y.; Brozena, A. H.; Cullen, D. A.; Chi, M.; Blum, T. F.; Morris, D.; Finfrock, Z.; Wang, X.; Zhang, P.; Goncharov, V. G.; Guo, X.; Luo, J.; Mo, Y.; Jiao, F.; Hu, L., Multi-principal elemental intermetallic nanoparticles synthesized via a disorder-to-order transition. *Sci. Adv.* **2022,** *8*, eabm4322.
(27) Jia, Z.; Yang, T.; Sun, L.; Zhao, Y.; Li, W.; Luan, J.; Lyu, F.; Zhang, L. C.; Kruzic, J. J.; Kai, J. J.; Huang, J. C.; Lu, J.; Liu, C. T., A Novel Multinary Intermetallic as an Active Electrocatalyst for Hydrogen Evolution. *Adv. Mater.* **2020,** *32*, 2000385.
(28) Zhu, G.; Jiang, Y.; Yang, H.; Wang, H.; Fang, Y.; Wang, L.; Xie, M.; Qiu, P.; Luo, W., Constructing Structurally Ordered High-entropy Alloy Nanoparticles on Nitrogen-rich Mesoporous Carbon Nanosheets for High-performance Oxygen Reduction. *Adv. Mater.* **2022,** *34*, 2110128.
(29) Zhao, K.; Li, X.; Su, D., High-Entropy Alloy Nanocatalysts for Electrocatalysis. *Acta Phys. Chim. Sin* **2021,** *37*, 2009077.
(30) Ma, Y.; Ma, Y.; Wang, Q.; Schweidler, S.; Botros, M.; Fu, T.; Hahn, H.; Brezesinski, T.; Breitung, B., High-entropy energy materials: challenges and new opportunities. *Energy Environ. Sci.* **2021,** *14*, 2883-2905.
(31) Yao, Y.; Dong, Q.; Brozena, A.; Luo, J.; Miao, J.; Chi, M.; Wang, C.; Kevrekidis, I. G.; Ren, Z. J.; Greeley, J.; Wang, G.; Anapolsky, A.; Hu, L., High-entropy nanoparticles: Synthesis-structure-property relationships and data-driven discovery. *Science* **2022,** *376*, eabn3103.
(32) Wang, Z.; Gu, Y.; Zheng, L.; Hou, J.; Zheng, H.; Sun, S.; Wang, L., Machine Learning Guided Dopant Selection for Metal Oxide-Based Photoelectrochemical Water Splitting: The Case Study of Fe2 O3 and CuO. *Adv. Mater.* **2021,** *34*, 2106776.
(33) Chun, H.; Lee, E.; Nam, K.; Jang, J.-H.; Kyoung, W.; Noh, S. H.; Han, B., First-principle-data-integrated machine-learning approach for high-throughput searching of ternary electrocatalyst toward oxygen reduction reaction. *Chem Catal.* **2021,** *1*, 855-869.
(34) Gao, Q.; Pillai, H. S.; Huang, Y.; Liu, S.; Mu, Q.; Han, X.; Yan, Z.; Zhou, H.; He, Q.; Xin, H.; Zhu, H., Breaking adsorption-energy scaling limitations of electrocatalytic nitrate reduction on intermetallic CuPd nanocubes by machine-learned insights. *Nat. Commun.* **2022,** *13*, 2338.
(35) Mai, H.; Le, T. C.; Chen, D.; Winkler, D. A.; Caruso, R. A., Machine Learning for Electrocatalyst and Photocatalyst Design and Discovery. *Chem. Rev.* **2022,** *122*, 13478-13515.
(36) Chen, L.; Zhang, X.; Chen, A.; Yao, S.; Hu, X.; Zhou, Z., Targeted design of advanced electrocatalysts by machine learning. *Chin. J. Catal.* **2022,** *43*, 11-32.
(37) Zhang, X.; Tian, Y.; Chen, L.; Hu, X.; Zhou, Z., Machine Learning: A New Paradigm in Computational Electrocatalysis. *J. Phys. Chem. Lett.* **2022,** *13*, 7920-7930.
(38) Xie, T., Deep learning methods for the design and understanding of solid materials. *Diss. Massachusetts Institute of Technology* **2020**.
(39) Jain, A.; Ong, S. P.; Hautier, G.; Chen, W.; Richards, W. D.; Dacek, S.; Cholia, S.; Gunter, D.; Skinner, D.; Ceder, G., Commentary: The Materials Project: A materials genome approach to accelerating materials innovation. *APL mater.* **2013,** *1*, 011002.
(40) Strasser, P.; Koh, S.; Anniyev, T.; Greeley, J.; More, K.; Yu, C.; Liu, Z.; Kaya, S.; Nordlund, D.; Ogasawara, H.; Toney, M. F.; Nilsson, A., Lattice-strain control of the activity in dealloyed core-shell fuel cell catalysts. *Nat. Chem.* **2010,** *2*, 454-60.
(41) Li, G.; Yang, Q.; Manna, K.; Fu, C.; Deniz, H.; Jena, J.; Li, F.; Parkin, S.; Auffermann, G.; Sun, Y., Optimization of catalytic active sites in non-collinear antiferromagnetic Mn3Pt bulk single-crystal. *Mater. Today Phys.* **2019,** *10*, 100137.
(42) Yao, Y.; Huang, Z.; Xie, P.; Lacey, S. D.; Jacob, R. J.; Xie, H.; Chen, F.; Nie, A.; Pu, T.; Rehwoldt, M.; Yu, D.; Zachariah, M. R.; Wang, C.; Shahbazian-Yassar, R.; Li, J.; Hu, L., Carbothermal shock synthesis of high-entropy-alloynanoparticles. *Science* **2018,** *359*.